SPECTRUM OF ENGINEERING SCIENCES
ISSN (E) 3007-3138 (P) 3007-312X VOLUME 4, ISSUE 3, 2026

QUANTUM CONFINEMENT EFFECTS IN SEMICONDUCTOR NANOPARTICLES: A FIRST-PRINCIPLES STUDY OF ELECTRONIC AND OPTICAL PROPERTIES

Ghulam Abbas[*1], Sajid Nawaz[2], Shah Wali Ullah[3], Ghufran Ur Rehman[4]

[*1] *Department of Physics, University of Southern Punjab, Multan, Pakistan*
[2] *Institute of Physics, Bahauddin Zakariya University, Multan, Pakistan*
[3] *Ph.D. Student, Advanced Functional Materials (AFM) Laboratory, Engineering Physics Department, Institute of Technology Bandung, Bandung 40132, Indonesia*
[4] *Pak-Austria Fachhochschule Institute of Applied Sciences and Technology, Pakistan*

[*1]abbas9017544@gmail.com, [2]sajidnawaz5121472@gmail.com, [3]33323751@mahasiswa.itb.ac.id, [4]ghufran_rehman@live.com

DOI: https://doi.org/10.5281/zenodo.23937124

Keywords
quantum confinement; semiconductor nanoparticles; quantum dots; effective-mass theory; finite potential barrier; exciton; Coulomb interaction; optical absorption; CdSe; electronic structure.

Article History
Received: 01 January 2026
Accepted: 16 March 2026
Published: 31 March 2026

Copyright @Author
Corresponding Author: *
Ghulam Abbas

Abstract

When the diameter of a semiconductor particle falls below the Bohr diameter of its exciton, the optical gap and the spectrum of electronic levels depend on particle size, and the material can be tuned across the visible and near-infrared range without changing its composition. In this article we study confinement in spherical nanoparticles of CdS, CdSe, CdTe, ZnSe and InP by solving the quantum-mechanical envelope-function problem directly. Single-particle states are obtained for a finite spherical well with an energy-dependent effective mass and a Ben Daniel–Duke boundary condition, and the electron–hole Coulomb attraction is added to first order from the computed wavefunctions. No atomistic calculation was performed. The inputs are bulk band-edge parameters from the literature, and only two quantities were chosen with reference to experiment: a barrier height of 2 eV and the use of static screening, both selected against one published CdSe sizing curve. For CdSe the lowest transition moves from 1.83 eV (676 nm) at 8 nm to 2.73 eV (455 nm) at 2 nm. At 4 nm the electron and hole confinement energies are 0.30 and 0.15 eV and the Coulomb term lowers the transition by 0.11 eV, or 24% of the confinement energy. Treating the barrier as infinite overestimates the size-induced shift by 68 to 86% between 3 and 6 nm, because about 4% of the electron density of a 4 nm particle lies outside it. Against the experimental curve the model has a root-mean-square deviation of 47 meV, with errors below 43 meV up to a diameter of 3.3 nm and an underestimate of up to 73 meV between 5.6 and 7 nm. The spectral sensitivity reaches 41 nm per nm of diameter for CdSe at 4 nm, so a 5% size dispersion alone broadens the lowest transition by about 19 nm. We state which conclusions this level of theory can support, give a reporting checklist, and outline the atomistic first-principles calculations that would test the remaining discrepancies.

1. INTRODUCTION

1.1 Background and motivation

Early observations of size-dependent absorption were made on CuCl microcrystals grown in silicate glass, where the position of the exciton line moved to higher energy as the crystals became smaller [1, 2]. The effect was explained at the same time as the quantum motion of an electron and a hole inside a sphere [3], and it was soon seen in colloidal CdS, where the absorption edge moved to higher energy as the particles were made smaller [4]. Brus then gave a compact expression for the lowest excited state that joined the kinetic energy of confinement to the electron–hole Coulomb attraction [5]. These results established the picture that is still used to interpret nanocrystal spectra: a particle smaller than the exciton Bohr diameter behaves as an artificial atom with discrete levels whose spacing is controlled by its size [6–8].

The picture became practical when synthetic chemistry produced nearly monodisperse samples. The hot-injection route for CdS, CdSe and CdTe gave particles with a size dispersion of a few per cent, and with it absorption spectra that resolve several excited transitions [9]. A detailed assignment of these transitions required the valence-band structure to be included [10, 11]. Since then the same physical idea has been applied in light-emitting devices [12], optical gain media [13], biological labels [14] and, for silicon, in the visible luminescence of nanostructured material [15]. Recent reviews describe the field as moving from the study of single materials towards engineered heterostructures and devices [16–18].

For these applications the quantity that matters is the transition energy as a function of size, together with the strength and spacing of the higher transitions. A designer who wants emission at a given wavelength needs the particle diameter, the sensitivity of the wavelength to diameter errors, and an estimate of how much the surrounding medium changes the result. Because confinement is a consequence of the Schrödinger equation, these questions can be answered from first principles of quantum mechanics, but the level at which the calculation is done determines what can be trusted. The simplest treatments use the bulk effective mass and an infinite barrier [3, 5]. Atomistic treatments describe the particle atom by atom but are limited in size and, in the case of density functional theory, in the accuracy of the gap [19–21].

1.2 Problem statement

Two difficulties recur when confinement results are compared across materials and studies. First, the infinite-barrier approximation is convenient but overestimates confinement energies, and the size of the error depends on the carrier mass and on the surrounding medium, which are rarely stated together with the result [22, 23]. Second, the energy of the electron–hole Coulomb term depends on a choice of dielectric constant that varies between papers, which changes the predicted gap by tens of millielectronvolts at diameters of 4 to 6 nm. As a result, a calculated gap and a measured gap can differ by an amount that is comparable to the size effect being studied, and it is not clear whether the difference comes from the model, the parameters or the sample.

1.3 Research gap

Reviews of nanocrystal electronic structure give the theory in detail [7, 11], and sizing curves relate the measured absorption peak to the diameter for several materials [24]. What is missing is a single, consistent calculation in which several materials are treated with the same boundary conditions, the same barrier and the same treatment of the Coulomb term, so that differences between materials can be attributed to their band parameters. A second gap concerns the stated accuracy: calculations are often compared with experiment at one size or for one material, so the trend of the error with diameter is not seen. A third is the status of the word first-principles. It is used for calculations that solve the Schrödinger equation without empirical fitting to size-dependent data, but it is also used for calculations based on density functional theory [25, 26]. The two meanings are not equivalent and the distinction affects what the results mean.

1.4 Objectives and research questions

The study has four objectives: (i) to set out the quantum-mechanical problem of a carrier in a finite spherical well with an energy-dependent mass, in a form that can be solved without further

approximation; (ii) to compute the single-particle levels, the electron–hole Coulomb energy and the optical transitions for CdS, CdSe, CdTe, ZnSe and InP over diameters from 2 to 10 nm; (iii) to quantify the errors caused by the infinite-barrier and parabolic-band approximations; and (iv) to compare the results with an experimental CdSe sizing curve and state where the model fails. We address three questions. RQ1: how is the size-induced shift divided between the electron, the hole and the Coulomb term, and how large is the error of the infinite-barrier model? RQ2: how well does a continuum model with bulk parameters reproduce the measured size dependence, and at which sizes does it fail? RQ3: which quantities control the spectral sensitivity to size, and what should be reported so that results can be compared?

1.5 Scope and organisation

The calculations treat spherical particles with a single conduction band and a single heavy-hole valence band. They do not include valence-band mixing, the electron–hole exchange interaction, surface states, shape anisotropy or dielectric mismatch. Section 2 reviews the theory of confinement, the exciton problem, the computational methods available and the experimental benchmarks. Section 3 describes the model, the parameters and the validation protocol. Section 4 presents the computed levels, gaps, energy decomposition, absorption spectra, spectral sensitivity, barrier sensitivity, the comparison with experiment, and spatial maps, parameter surfaces and an atomistic count for the particles. Section 5 discusses the findings against the research questions, lists the limitations and sets out future work, and Section 6 concludes.

2. Literature Review

2.1 Confinement of a carrier in a sphere

In the envelope-function description, the carrier near a band edge moves in a slowly varying potential, and its wavefunction is the product of the periodic Bloch function of the band edge and an envelope that obeys a Schrödinger equation with the effective mass [23, 27]. For a particle in an infinite spherical well of radius R the envelope has the form of a spherical Bessel function and the energies are $E_{nl} = \hbar^2\chi_{nl}^2/(2m^*R^2)$, where χ_{nl} is the nth zero of the spherical Bessel function of order l. The lowest state is l = 0 with $\chi = \pi$, the next is l = 1 with $\chi = 4.493$, and then l = 2 with $\chi = 5.763$ [3, 7]. Levels are labelled 1S, 1P, 1D, 2S and so on, and each has a degeneracy of 2l + 1 apart from spin. Figure 1a contrasts the resulting density of states with that of a bulk crystal, a quantum well and a quantum wire: each reduction in dimension replaces a smooth function by a series of steps, then by edge singularities, and finally by discrete lines [8].

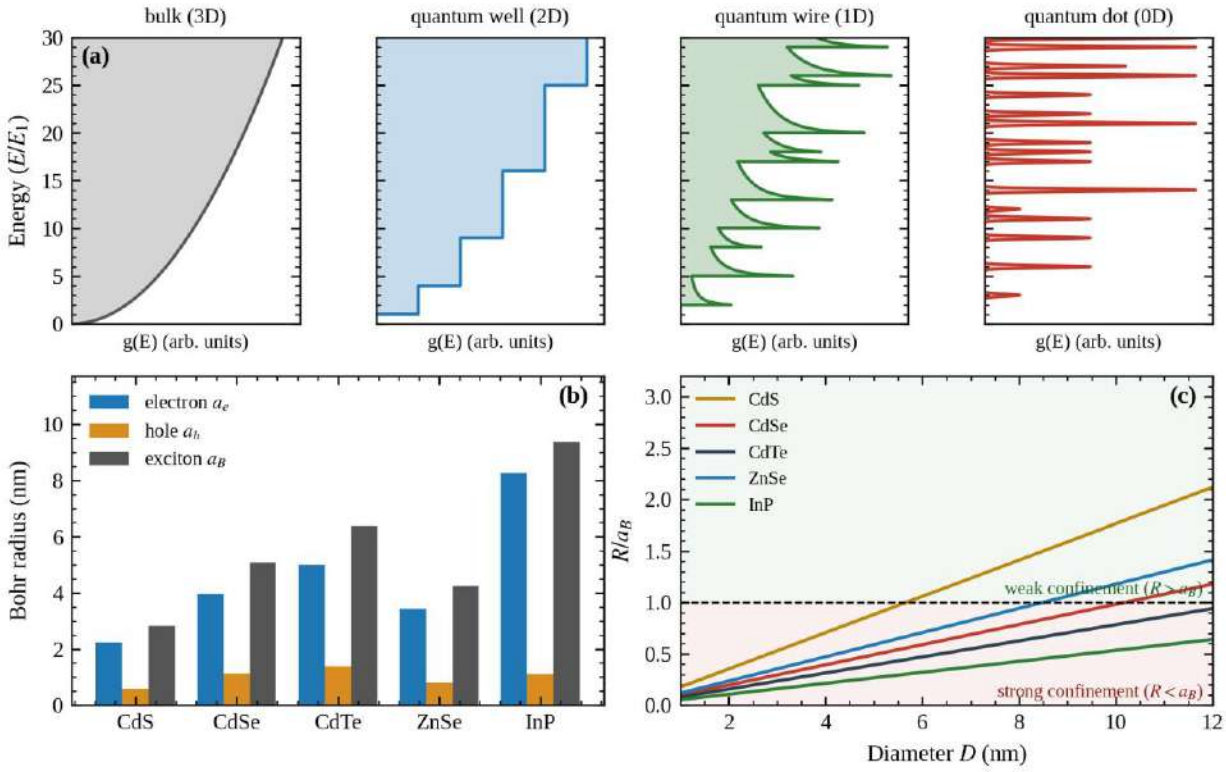


Figure 1. (a) Density of states for free carriers in bulk, in a quantum well, in a quantum wire and in a quantum dot, computed in units of the lowest confinement energy E_1 from the standard infinite-well expressions (the dot spectrum is shown with a Gaussian width of 0.12 E_1). (b) Electron, hole and exciton Bohr radii of the five materials, from the parameters of Table 3 with the static dielectric constant. (c) Ratio of particle radius R to exciton Bohr radius a_B as a function of diameter; the dashed line separates strong from weak confinement.

Real barriers are finite. A carrier that leaks into the surrounding medium is less confined, and its mass changes at the interface. The accepted boundary condition makes the envelope and the quantity ψ'/m continuous, which conserves probability current across an abrupt change of mass [22]. In narrow-gap materials the effective mass also depends on energy because the conduction and valence bands are coupled; in the two-band model of Kane this gives $E(1 + E/E_g) = \hbar^2k^2/(2m^*)$ [28]. Both corrections lower the confinement energy relative to the infinite, parabolic model, and both become more important as the particle becomes smaller.

2.2 Electron–hole interaction and confinement regimes

The electron and hole attract each other, and the competition between this attraction and the confinement defines the regime [29]. The exciton Bohr radius $a_B = 4\pi\varepsilon_0\varepsilon\,\hbar^2/(\mu e^2)$, with μ the reduced mass, sets the length scale. If the particle radius is much larger than a_B the exciton moves as a whole inside the particle and only its centre of mass is quantised (weak confinement). If the radius is much smaller than a_B the electron and hole are quantised separately and the Coulomb term is a perturbation that scales as $1/R$ (strong confinement). Between these limits, when the radius lies between the electron and hole Bohr radii, the lighter carrier is strongly confined while the heavier one is still bound to the Coulomb field

of the first [11, 29]. Brus summarised the strong-confinement limit with the expression $E \approx E_g + \hbar^2\pi^2/(2R^2)\ (1/m_e + 1/m_h) - 1.786\ e^2/(4\pi\varepsilon_0\varepsilon R)$, which is still the starting point for most size estimates [5].

The dielectric constant that enters the Coulomb term is not settled. The optical value describes screening by the electrons alone and suits carriers that move faster than the lattice; the static value includes lattice polarisation and suits states close to the band edge. Atomistic pseudopotential calculations of the exciton Coulomb and exchange energies show that the continuum treatment of screening is an approximation whose accuracy has to be checked, and that the electron–hole exchange interaction, which the Brus expression omits, splits the lowest exciton level [21].

2.3 Computational approaches

Four families of methods are used to compute nanocrystal levels. The envelope-function and k·p methods treat the particle as a continuum and need only a few bulk parameters; they are fast and transparent but cannot describe the atomic structure of the surface [7, 11]. Empirical tight-binding methods place orbitals on every atom and have been applied to silicon particles with up to thousands of atoms [30]. Empirical pseudopotentials with folded-spectrum or similar techniques give the states near the gap for particles with many thousands of atoms and include the electron–hole interaction directly [20, 21]. Finally, *ab initio* methods start from density functional theory [25, 26]. Kohn–Sham eigenvalue gaps with standard functionals are smaller than the quasiparticle gap because the exact functional has a derivative discontinuity [19]; screened hybrid functionals reduce the error [31], and the GW approximation with the Bethe–Salpeter equation gives quasiparticle and excitonic energies [32, 33], at a cost that limits the size of the system. Plane-wave codes widely used for these calculations are described in [34, 35]. Table 1 compares the approaches.

Table 1. Computational approaches to the electronic structure of semiconductor nanocrystals.

Method	Basis of the approach	Practical size range	Main strength	Main limitation
Effective mass / k·p	Continuum envelope with bulk band parameters	No atomic limit; any size	Transparent, fast, size trends	Surface, shape and atomic detail absent
Tight binding	Localised orbitals on every atom, fitted parameters	10^3 to 10^5 atoms	Atomistic, includes valence-band mixing	Parameters fitted to bulk bands; surface treatment empirical
Empirical pseudopotential	Screened atomic potentials fitted to bulk data	10^3 to 10^5 atoms	Direct exciton Coulomb and exchange	Needs transferable potentials for each material
Density functional theory	Kohn–Sham equations with an exchange–correlation functional	About 10^2 to 10^3 atoms routinely	No fitting to size-dependent data; relaxed surfaces	Gap underestimated with standard functionals; cost grows steeply with size
GW and Bethe–Salpeter	Many-body perturbation theory on a DFT starting point	About 10^2 atoms	Quasiparticle gaps and excitons	Very high cost; usually smaller particles than experiments

Size ranges are indicative orders of magnitude and depend on the code and the computing resources.

2.4 Experimental benchmarks

The most widely used benchmark is the dependence of the first absorption peak of CdSe on the diameter measured by electron microscopy. Yu and co-workers fitted a polynomial relating the peak wavelength to the diameter for CdSe, and similar relations for CdTe and CdS, over a range of about 2 to 7 nm [24]. Resolved excited-state transitions were assigned by Norris and Bawendi, who showed that the transitions do not follow the simple pairing of electron and hole levels with the same quantum numbers because the valence band mixes angular momentum states [10]. The consequence for the present work is that a single-band hole model can reproduce the first transition and the trend of the gap, but not the detailed order and intensity of the higher transitions.

2.5 Applications that depend on size control

Display and lighting applications need the emission wavelength to be reproducible from batch to batch, so the sensitivity of wavelength to diameter sets the required size control [12, 17]. Optical gain depends on the degeneracy and spacing of the band-edge levels, which are set by the confinement and by the Coulomb interaction [13]. Biological imaging needs sizes and surface chemistry that keep the particle small while preserving the optical properties [14]. Core–shell structures are used to reduce surface losses and, through the band offsets, to change the leakage of carriers outside the core [18]; this last point makes the finite-barrier problem studied here directly relevant to the design of such structures.

2.6 Synthesis of the literature and research gap

Table 2 collects representative studies and the questions they leave open for the present work. The pattern is that the physical ingredients (finite barrier, nonparabolicity, Coulomb correction) are individually known, but their relative sizes are not usually shown together for several materials on a common footing, and the trend of the error with diameter is not reported. The remainder of this article supplies such a comparison within a continuum model and states clearly which parts of the problem it cannot address.

Table 2. Representative studies and the questions they leave open for this work.

Study	Approach	Main finding	Open question
Efros and Efros [3]	Infinite spherical well, effective mass	Size-dependent interband absorption and strong/weak limits	Role of finite barrier and band nonparabolicity
Brus [5]	Variational / perturbative Coulomb correction	Compact expression for the lowest excited state	Accuracy at diameters above the strong-confinement limit
Kayanuma [29]	Electron–hole pair in a sphere over all regimes	Regimes set by R/a_B and the mass ratio	Application to several materials with a finite barrier
Norris and Bawendi [10]	Absorption and luminescence excitation of CdSe	Excited transitions assigned with valence-band mixing	Size of the error when mixing is neglected
Franceschetti and Zunger [21]	Pseudopotential calculation of exciton energies	Coulomb and exchange energies from atomistic wavefunctions	Comparison with the continuum Coulomb term
Yu *et al.* [24]	Sizing curves from measured spectra	Peak wavelength to diameter relation for CdSe, CdTe and CdS	Test of continuum models along the whole curve

3. Methodology

3.1 Research design

The study is a computational investigation based on the quantum-mechanical solution of the envelope-function problem. It has three parts: the calculation of single-particle levels and wavefunctions in a finite spherical well; the calculation of the electron–hole Coulomb energy and the optical transitions from those wavefunctions; and a comparison of the result with an experimental sizing curve. No synthesis or measurement was carried out, and no atomistic calculation, whether density functional theory or tight binding, was performed. The word first-principles is therefore used in the restricted sense that the size dependence is obtained from the Schrödinger equation with bulk band parameters and without fitting to size-dependent data, except for the two choices described in Section 3.6. Quantities taken from the literature and quantities computed here are distinguished throughout.

3.2 Model Hamiltonian

Electrons in the conduction band and holes in the heavy-hole valence band are described by separate envelope functions $\psi(\mathbf{r})$. Each satisfies

$$[\,-(\hbar^2/2)\nabla\cdot(1/m(\mathbf{r}))\,\nabla + V(\mathbf{r})\,]\,\psi(\mathbf{r}) = E\,\psi(\mathbf{r}), \quad (1)$$

where $m(\mathbf{r})$ equals the effective mass m^* inside the particle (radius R) and $m_b = m_0$ outside, and $V(\mathbf{r})$ is zero inside and V_0 outside. Energies are measured from the relevant bulk band edge, upward for electrons and downward for holes. The surrounding medium is represented by a vacuum-like mass and a rectangular barrier, a simplification discussed in Section 5.6. The solutions separate as $\psi = u(r)/r \cdot Y_{lm}(\theta, \varphi)$, and for each angular momentum l the radial problem is solved separately.

3.3 Radial solution with a finite barrier

Inside the particle the radial function is a spherical Bessel function $j_l(kr)$ and outside it is a modified spherical Bessel function of the second kind, $k_l(\kappa r)$, which decays. The wave numbers are related to the energy by

$$\hbar^2k^2/(2m^*) = E(1 + E/E_g), \quad \kappa = [2m_b(V_0 - E)]^{1/2}/\hbar, \quad (2)$$

where the first relation is the two-band Kane dispersion [28] and E_g is the bulk gap. Continuity of the envelope and of ψ'/m at $r = R$ [22] gives the eigenvalue condition

$$[k/m_w(E)]\, j'_l(kR)\, k_l(\kappa R) - (\kappa/m_b)\, j_l(kR)\, k'_l(\kappa R) = 0, \quad (3)$$

with $m_w(E) = m^*(1 + 2E/E_g)$, the velocity mass derived from the Kane dispersion. For a parabolic band the factor in brackets is replaced by m^*. The condition is written in the product form of Eq. (3) so that it has no poles. Its roots were found by scanning the interval $0 < E < V_0$ on a grid of 3000 points for sign changes and refining each by Brent's method; every root was checked to be a zero of the function and not a discontinuity. The root finder was tested against an independent finite-difference solution of Eq. (1) written for the radial function $\psi(r)$ on a grid of 60 000 points, which enforces the same boundary condition without the Bessel-function matching. For $l = 0$, 1 and 2, for masses of 0.13 and 0.45 m_0 inside and m_0 outside, and for radii of 1 to 3 nm, the two methods agree to within 0.2 meV (for example 0.2887 and 0.2888 eV for the 1S electron level at $R = 2$ nm and $V_0 = 2$ eV). With $V_0 \to \infty$ and a parabolic band the code returns the analytic result $E = \hbar^2\chi_{nl}^2/(2m^*R^2)$. The normalised radial functions were then constructed by matching the interior and exterior solutions at R.

3.4 Electron–hole Coulomb energy

The Coulomb attraction between an electron and a hole in the states (n, l) was computed to first order in the interaction, using the monopole term of the multipole expansion:

$$E_C = (e^2/4\pi\varepsilon_0\varepsilon) \iint u_e^2(r_1)\, u_h^2(r_2) / \max(r_1, r_2)\, dr_1\, dr_2, \quad (4)$$

where ε is the static dielectric constant of the particle. The double integral was evaluated by cumulative trapezoidal integration on a grid of 4000 points extending to three radii. In the infinite-barrier limit this expression gives the $1.786\, e^2/(4\pi\varepsilon_0\varepsilon R)$ of Brus [5], which is used for the infinite-barrier comparison. Dielectric mismatch between particle and medium, which produces polarisation self-energies that nearly cancel in the

electron–hole pair [5], and the electron–hole exchange interaction are neglected. The transition energy of a pair is

$$E_{pair} = E_g + E_e + E_h - E_C. \quad (5)$$

3.5 Optical transitions

Optical transitions connect an electron level and a hole level of the same angular momentum l. In the single-band picture used here the relative strength of a transition is taken as

$$f \propto (2l + 1) \, | \int u_e(r) \, u_h(r) \, dr \, |^2, \quad (6)$$

the overlap of the radial functions multiplied by the number of degenerate pairs. The factor $(2l + 1)$ is a property of the model and not a measured intensity. Absorption spectra were built by placing a Gaussian of 35 meV standard deviation at each transition above a relative strength of 0.01 and averaging over a Gaussian distribution of diameters with a relative standard deviation of 5%, sampled at eleven points between ±2.5 standard deviations. Transitions with $l \le 3$ and up to three radial states were included, so the spectrum becomes incomplete above about 4 eV.

3.6 Material parameters, barrier and screening

Band-edge parameters (Table 3) are representative values for room temperature taken from standard compilations [36, 37]. Heavy-hole masses were used for the valence band; this is a simplification, because the hole mass in wurtzite and zinc-blende materials depends on direction and on the valence-band subband. The same barrier height, V_0 = 2.0 eV, and the same outer mass, m_0, were used for electrons and holes in all materials, so that differences between materials come from their band parameters alone. Two choices were fixed by comparison with experiment: the barrier height and the use of the static, instead of the optical, dielectric constant in the Coulomb term. They were selected by scanning V_0 from 1 to 5 eV with both dielectric constants against the CdSe sizing curve described in Section 3.7, and the pair with the smallest root-mean-square deviation (V_0 = 2 eV, static) was kept. The agreement shown for CdSe is therefore a calibration, not an independent test, and the results for the other four materials are predictions of the calibrated model that have not been compared with experiment here.

Table 3. Parameters of the five materials and derived Bohr radii.

Material	E_g (eV)	m_e/m_0	m_h/m_0	ε_∞	ε_s	μ/m_0	a_e (nm)	a_h (nm)	a_B (nm)	Ry^* (meV)
CdS	2.42	0.21	0.80	5.2	8.9	0.166	2.24	0.59	2.83	28.6
CdSe	1.74	0.13	0.45	6.2	9.7	0.101	3.95	1.14	5.09	14.6
CdTe	1.50	0.11	0.40	7.2	10.4	0.086	5.00	1.38	6.38	10.9
ZnSe	2.70	0.14	0.60	5.9	9.1	0.114	3.44	0.80	4.24	18.7
InP	1.35	0.08	0.60	9.6	12.5	0.071	8.27	1.10	9.37	6.1

Representative literature values [36, 37]. $a_e = 4\pi\varepsilon_0\varepsilon_s\hbar^2/(m_e e^2)$, a_h likewise, a_B with the reduced mass μ, and $Ry^* = 13.606 \text{ eV} \times \mu/(m_0\varepsilon_s^2)$. Computed in this work.

3.7 Experimental comparison

The comparison is made with the sizing relation of Yu *et al.* for CdSe, which gives the diameter D (nm) from the wavelength λ (nm) of the first absorption peak as $D = 1.6122 \times 10^{-9}\lambda^4 - 2.6575 \times 10^{-6}\lambda^3 + 1.6242 \times 10^{-3}\lambda^2 - 0.4277\lambda + 41.57$ [24]. The relation was evaluated at nine wavelengths from 480 to 640 nm in steps of 20 nm. The points in the figures are therefore values of a published fit and not raw measurements, and they carry the uncertainty of the underlying diameters, which come from electron microscopy of the samples used in that study. The model was compared in energy, $E = 1239.84/\lambda$ (eV with λ in nm), and, by inverting the model, in diameter.

3.8 Spectral sensitivity and size dispersion

The sensitivity of the transition wavelength to diameter was calculated as $d\lambda/dD$ by numerical differentiation of the computed gap-versus-size

curve. The inhomogeneous broadening produced by a diameter distribution of standard deviation σ_D is, to first order, $\sigma_\lambda = |d\lambda/dD|\ \sigma_D$, FWHM = 2.355 σ_λ. (7)

The local exponent of the size dependence, $\alpha = -d \ln \Delta E / d \ln D$, with ΔE the shift of the lowest transition from the bulk gap, was used to compare the computed trend with the $1/D^2$ scaling of the infinite well and the $1/D$ scaling of the Coulomb term.

3.9 Implementation

All calculations were done in Python 3 with NumPy and SciPy (spherical Bessel functions and Brent root finding) and the figures with Matplotlib. The lowest transition of a particle takes a fraction of a second on a single processor core, and the full set of figures can be regenerated in a few minutes. The scripts are available from the corresponding author on request.

4. Results

4.1 Confinement regimes

Table 3 and Figure 1b,c give the length scales that decide the regime. The electron Bohr radius ranges from 2.2 nm in CdS to 8.3 nm in InP, while the hole Bohr radius is between 0.6 and 1.4 nm in all five materials, because the heavy-hole mass is between 3.5 and 7.5 times the electron mass. The exciton Bohr radius a_B with static screening is 2.8 nm for CdS, 4.2 nm for ZnSe, 5.1 nm for CdSe, 6.4 nm for CdTe and 9.4 nm for InP. A particle is below the strong-confinement threshold $R = a_B$ at diameters of 5.7, 8.5, 10.2, 12.8 and 18.7 nm for the same five materials. For CdSe at 4 nm, $R = 2.0$ nm is smaller than a_e but larger than $a_h = 1.1$ nm, so the system belongs to the intermediate regime in which the hole is only moderately confined [29]. This has a consequence for the accuracy of a perturbative Coulomb term that is discussed in Section 5.3.

4.2 Single-particle levels and wavefunctions

Figure 2a shows the levels of a 4 nm CdSe particle. The electron levels are spaced much further apart than the hole levels: the 1P–1S spacing is 0.32 eV for the electron and 0.14 eV for the hole, in the ratio of about 2.3 that is expected from the mass ratio of 3.5 reduced by the nonparabolicity and the finite barrier. The energies of the first six levels at three diameters are given in Table 4. The electron 1S level moves from 0.44 eV at 3 nm to 0.30 eV at 4 nm and 0.17 eV at 6 nm. At 2 nm only the electron levels 1S and 1P are bound below the 2 eV barrier, which sets a lower limit on the size range in which a two-level or higher description can be used.

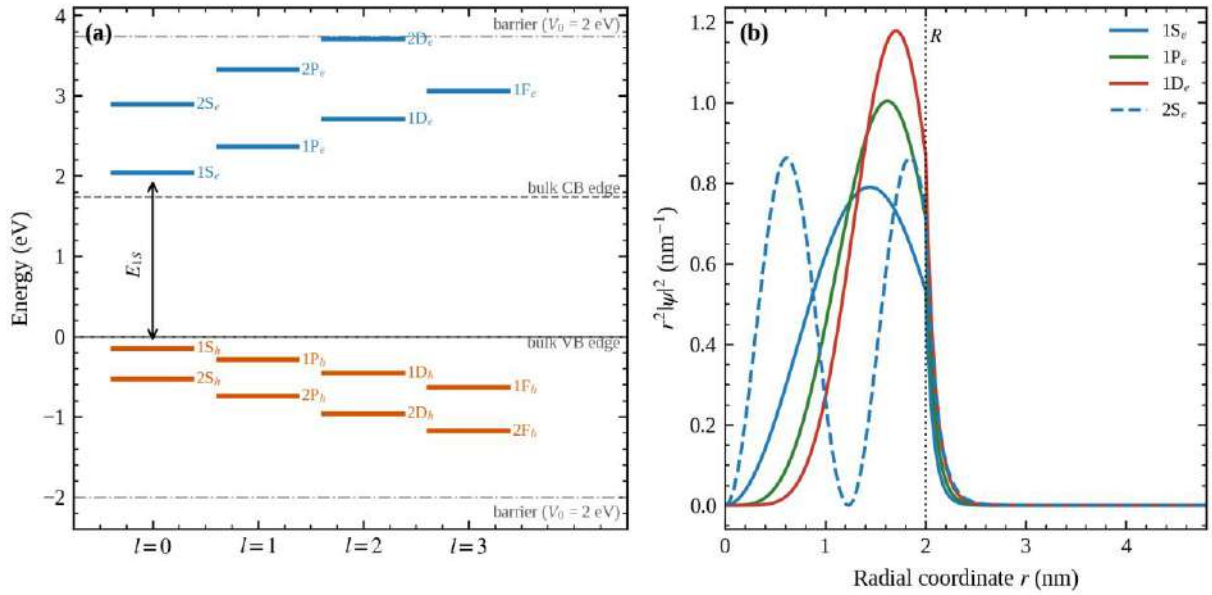


Figure 2. (a) Electron (blue) and hole (orange) levels of a 4 nm CdSe particle with a barrier of 2 eV, measured from the bulk band edges. The arrow marks the lowest pair transition before the Coulomb correction. (b) Radial probability densities $r^2|\psi|^2$ of the electron states 1S, 1P, 1D and 2S. The dotted line marks the particle radius R = 2 nm.

Table 4. Single-particle energies (eV) of CdSe particles with V_0 = 2 eV, measured from the bulk band edges.

State	D = 3 nm, electron	D = 3 nm, hole	D = 4 nm, electron	D = 4 nm, hole	D = 6 nm, electron	D = 6 nm, hole
1S	0.438	0.238	0.296	0.149	0.166	0.074
1P	0.912	0.460	0.620	0.291	0.344	0.147
1D	1.387	0.704	0.969	0.455	0.550	0.234
1F	1.830	0.960	1.320	0.631	0.771	0.332
2S	1.635	0.810	1.152	0.528	0.657	0.275
2P	not bound	1.116	1.579	0.744	0.933	0.397

Computed in this work. The label "not bound" means that no solution exists below the barrier.

The wavefunctions in Figure 2b show that the 1S electron density peaks near 1.4 nm and that the density of the 1P and 1D states is pushed towards the surface. All of them extend beyond the interface. The 2S state has a node at 1.2 nm. The tail outside the particle is longer for states of higher energy because they lie closer to the top of the well. This leakage is quantified in Section 4.7.

4.3 Optical gap as a function of size

Figure 3a shows the lowest transition energy of the five materials between 2 and 10 nm, and Table 5 lists values at selected sizes. All curves approach the bulk gap from above and become flat above about 8 nm. For CdSe the transition is 2.73 eV at 2 nm, 2.28 eV at 3 nm, 2.08 eV at 4 nm, 1.97 eV at 5 nm, 1.91 eV at 6 nm and 1.83 eV at 8 nm, corresponding to wavelengths of 455, 544, 597, 629, 651 and 676 nm. The range of wavelengths that can be reached by varying the diameter from

2 to 8 nm is 221 nm for CdSe, 110 nm for CdS, 101 nm for ZnSe, 284 nm for CdTe and 320 nm for InP.

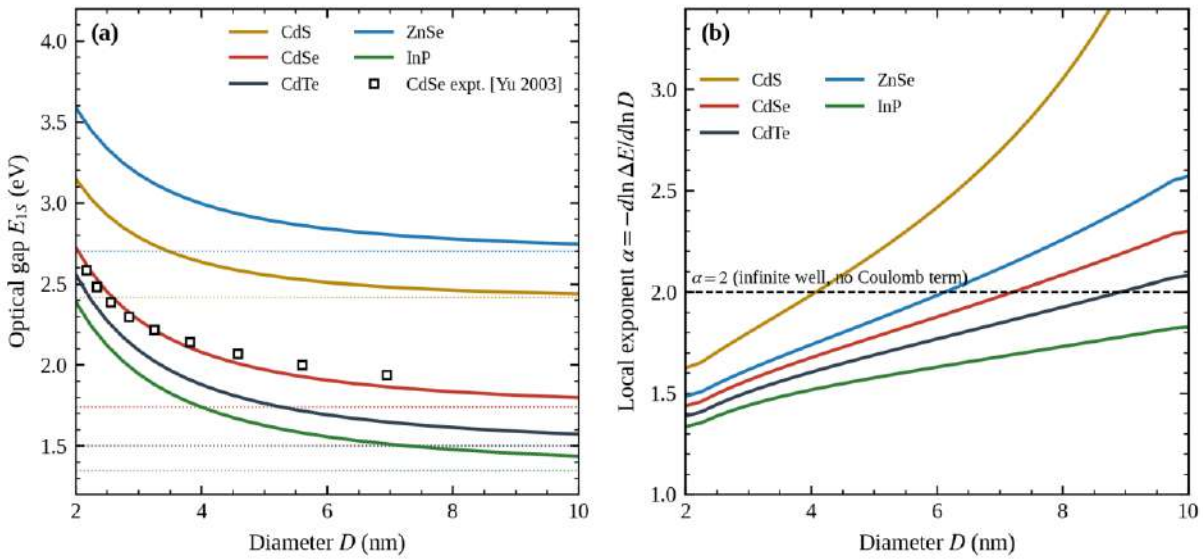


Figure 3. (a) Computed lowest transition energy as a function of diameter for five materials. Dotted lines are the bulk gaps. Open squares show the CdSe sizing relation of Yu *et al.* [24] evaluated at nine wavelengths. (b) Local exponent $\alpha = -\mathrm{d}\ln \Delta E/\mathrm{d}\ln D$ of the shift from the bulk gap. The dashed line marks $\alpha = 2$, the exponent of an infinite well without a Coulomb term.

Table 5. Lowest transition energy (eV) and wavelength (nm) of the five materials as a function of diameter.

D (nm)	CdS	CdSe	CdTe	ZnSe	InP
2	3.149 (394)	2.725 (455)	2.557 (485)	3.588 (346)	2.391 (519)
3	2.787 (445)	2.278 (544)	2.091 (593)	3.176 (390)	1.945 (637)
4	2.633 (471)	2.078 (597)	1.878 (660)	2.994 (414)	1.739 (713)
5	2.554 (485)	1.970 (629)	1.762 (704)	2.897 (428)	1.625 (763)
6	2.508 (494)	1.905 (651)	1.691 (733)	2.839 (437)	1.556 (797)
8	2.461 (504)	1.834 (676)	1.612 (769)	2.776 (447)	1.477 (839)
Bulk	2.420 (512)	1.740 (713)	1.500 (827)	2.700 (459)	1.350 (918)

Computed in this work with $V_0 = 2$ eV, Kane mass and static screening. Wavelengths in parentheses.

The exponent α in Figure 3b shows that the size dependence is not a simple power law. For CdSe it is 1.5 at 2.5 nm, 1.7 at 4 nm, 1.9 at 6 nm and 2.1 at 8 nm. At small size the leakage into the barrier and the Kane nonparabolicity both reduce the exponent below 2. At large size the Coulomb term, which falls as $1/D$, removes a growing fraction of the confinement energy, and the net shift decays faster than $1/D^2$. The effect is largest where the Coulomb energy is a large fraction of the confinement energy: the exponent for CdS reaches 3.0 at 8 nm, whereas InP, whose Bohr radius is large and whose Coulomb term is screened by $\varepsilon_s = 12.5$, stays below 1.8 up to 8 nm. A single-power fit to experimental gaps over a wide range of sizes would therefore return an exponent that depends on the range chosen.

4.4 Decomposition of the confinement shift

Figure 4 and Table 6 divide the shift of CdSe into electron confinement, hole confinement and Coulomb attraction. At 4 nm the electron contributes 0.296 eV, the hole 0.149 eV and the Coulomb term removes 0.107 eV, so that the net shift is 0.338 eV. The electron supplies 66% of the total confinement energy (0.296 of 0.445 eV) and the hole 34%. The ratio of the electron to the hole contribution rises from 1.6 at 2 nm to 2.6 at 10 nm; it is smaller than the mass ratio of 3.5 because the lighter carrier is the one most reduced by leakage and by the nonparabolicity. The Coulomb energy falls more slowly than the confinement energy, and its ratio to the sum of the confinement energies grows from 17% at 2 nm to 24% at 4 nm, 31% at 6 nm and 45% at 10 nm. At 10 nm the electron–hole attraction is 47 meV, which is more than three times the bulk exciton binding energy of 14.6 meV, so the particle has not yet reached the weak-confinement limit.

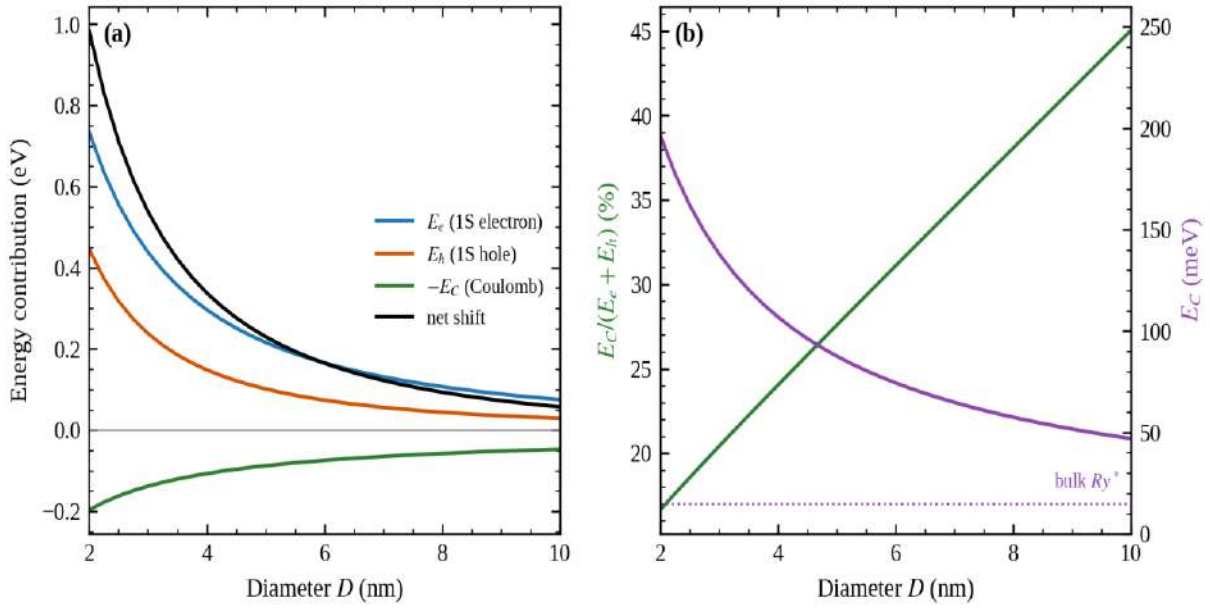


Figure 4. (a) Contributions to the lowest transition of CdSe: electron confinement energy E_e, hole confinement energy E_h, Coulomb term $-E_C$ and their sum. (b) Ratio of the Coulomb energy to the sum of the confinement energies (left axis) and Coulomb energy in meV (right axis); the dotted line is the bulk exciton Rydberg Ry^* = 14.6 meV.

Table 6. Contributions to the lowest transition of CdSe (eV).

D (nm)	E_e	E_h	E_C	E_{1S}	$E_C/(E_e + E_h)$ (%)
2	0.735	0.446	0.197	2.725	16.6
3	0.438	0.238	0.138	2.278	20.4
4	0.296	0.149	0.107	2.078	24.0
5	0.216	0.102	0.088	1.970	27.6
6	0.166	0.074	0.074	1.905	31.1
8	0.107	0.044	0.057	1.834	38.1
10	0.075	0.029	0.047	1.797	45.0

Computed in this work. $E_{1S} = E_g + E_e + E_h - E_C$ with E_g = 1.74 eV.

4.5 Absorption spectrum

The spectra in Figure 5a have the characteristic pattern of a series of peaks that move apart and to higher energy as the diameter decreases. For a 4 nm particle the first transitions are $1S_e1S_h$ at 2.08 eV, $1P_e1P_h$ at 2.56 eV, $1D_e1D_h$ at 3.08 eV, $2S_e2S_h$ at 3.30 eV and $1F_e1F_h$ at 3.61 eV. The spacing between the first two transitions is 0.71 eV at 3 nm, 0.48 eV at 4 nm and 0.26 eV at 6 nm (Table 7), so at 6 nm it is still more than seven times the 35 meV homogeneous width and the first peaks remain resolved at the 5% dispersion used in Figure 5a. The transition energies in Figure 5b fan out with decreasing diameter, as in the experimental spectra of CdSe [10].

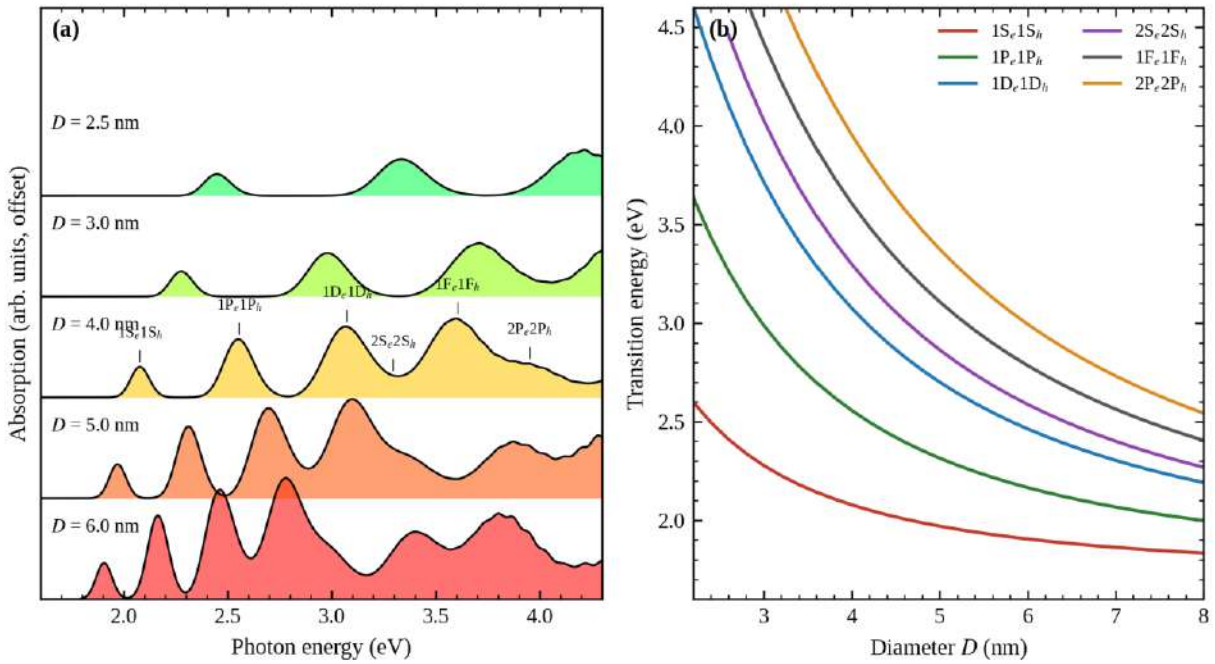


Figure 5. (a) Model absorption spectra of CdSe particles of five sizes, with a 5% standard deviation of the diameter and a homogeneous width of 35 meV; the colour of each curve is the colour of its lowest transition. The labels mark the transitions of the 4 nm particle. (b) Transition energies of the paired electron and hole states as functions of diameter.

Table 7. Pair transition energies (eV) of CdSe, including the Coulomb correction.

Transition	D = 3 nm	D = 4 nm	D = 6 nm
$1S_e1S_h$	2.278	2.078	1.905
$1P_e1P_h$	2.989	2.557	2.166
$1D_e1D_h$	3.716	3.075	2.463
$2S_e2S_h$	4.029	3.297	2.588
$1F_e1F_h$	4.422	3.606	2.784

Computed in this work. Only transitions between electron and hole states with the same quantum numbers are listed.

The calculated relative strengths (Eq. 6) rise with l, from 0.94 for 1S to 2.8 for 1P and 4.7 for 1D, because the degeneracy factor grows and the overlap of the electron and hole radial functions

stays close to 0.97. This ratio is a property of a single-band model. In real particles the mixing of valence-band states changes both the order and the intensity of the transitions [10, 11], and the results of this section should be read as the pattern of level spacings and not as predicted intensities.

4.6 Spectral sensitivity and size dispersion

The derivative dλ/dD, shown in Figure 6b, decreases rapidly with size. For CdSe it is 88 nm per nm at 2.5 nm, 41 at 4 nm, 18 at 6 nm and 9 at 8 nm. The other materials follow the same trend with different magnitudes: at 4 nm the values are 19 nm per nm for CdS, 18 for ZnSe, 53 for CdTe and 61 for InP. Materials with a narrower bulk gap are more sensitive because a given energy shift corresponds to a larger shift in wavelength. Equation (7) converts these values into a linewidth. A 5% distribution of the diameter (σ_D = 0.2 nm at 4 nm) gives σ_λ = 8 nm and a full width at half maximum of 19 nm for the lowest transition of CdSe, before any homogeneous broadening is added. At 6 nm the same relative dispersion (σ_D = 0.3 nm) gives 5.3 nm and 12.5 nm. Because dλ/dD falls with size, narrower lines for a given relative dispersion are expected for larger particles of the same material, and the diameter must be controlled to better than 0.1 nm in a 4 nm CdSe particle to keep the lowest transition within 4 nm of the target.

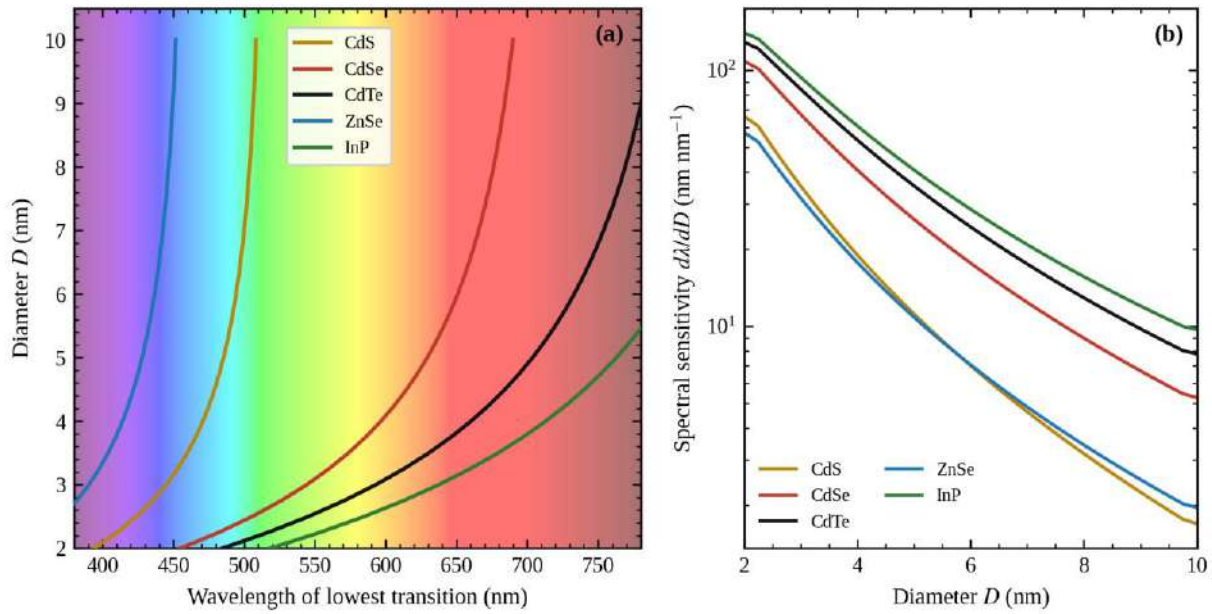


Figure 6. (a) Diameter needed to place the lowest transition at a given wavelength for five materials, drawn over the visible spectrum. (b) Spectral sensitivity dλ/dD of the lowest transition as a function of diameter. The colours in panel (a) are an approximate rendering of wavelength and are used only as a guide.

4.7 Sensitivity to the barrier and leakage

Figure 7a shows the effect of the barrier height on the lowest transition of CdSe. At 4 nm the transition is 2.006 eV for V_0 = 1 eV, 2.078 eV for 2 eV, 2.162 eV for 5 eV and 2.345 eV for an infinite barrier. The infinite-barrier shift from the bulk gap is therefore 0.605 eV, compared with 0.338 eV for the 2 eV barrier, an overestimate of 79%. At 3 nm the overestimate is 86% (0.998 against 0.538 eV) and at 6 nm it is 68% (0.277 against 0.165 eV). Changing the barrier between 1 and 5 eV moves the 4 nm transition by 0.156 eV and the 6 nm transition by 0.067 eV, so the uncertainty in the surrounding medium is a significant source of uncertainty in the prediction below 5 nm.

The corresponding probability that a carrier is found outside the particle is in Figure 7b. For the 1S electron at V_0 = 2 eV it is 11.9% at 2 nm, 6.4% at 3 nm, 4.0% at 4 nm, 1.9% at 6 nm and 0.66% at 10 nm. The hole, with its larger mass, has a probability of 3.7%, 1.6%, 0.87%, 0.33% and 0.08% at the same diameters. The electron therefore samples the surroundings between three and eight times more than the hole, the ratio growing with diameter,, which makes the electron level and the transition energy more sensitive to the shell or ligand than the hole level.

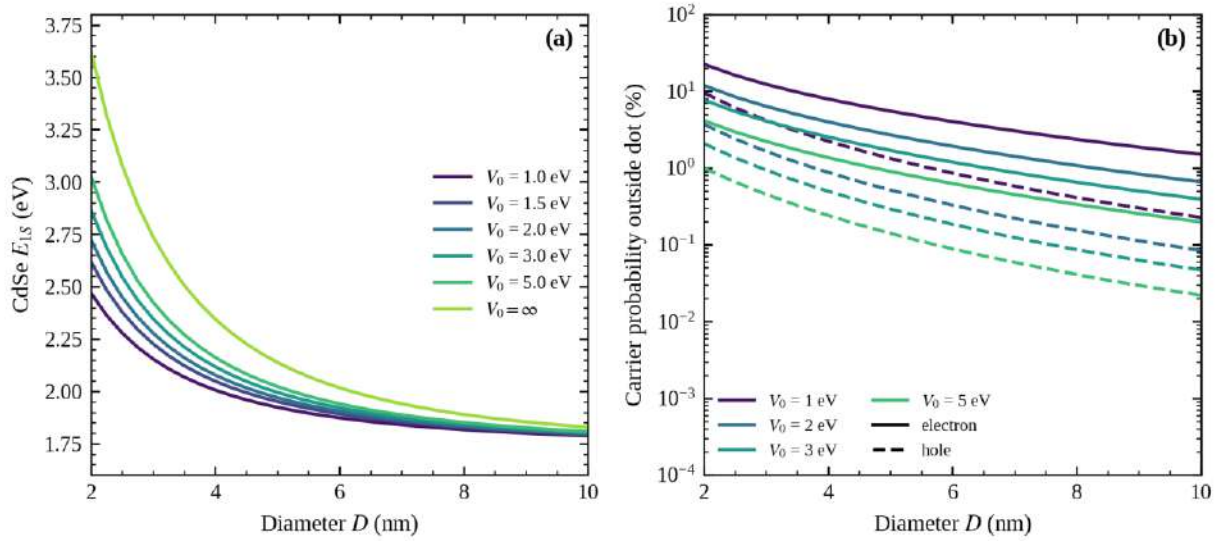


Figure 7. (a) Lowest transition of CdSe as a function of diameter for barrier heights from 1 eV to infinity (with Kane mass and Brus Coulomb term in the infinite case). (b) Probability of finding the 1S electron (solid) and the 1S hole (dashed) outside the particle for barrier heights of 1, 2, 3 and 5 eV.

Institute for Excellence in Education & Research

4.8 Comparison with the experimental sizing curve

Figure 8 and Table 8 compare the model with the sizing relation of Yu *et al.* [24]. In energy, the model overestimates the transition by 26 to 43 meV between 2.2 and 2.9 nm, agrees within 2 meV at 3.3 nm, and underestimates it by 33 meV at 3.8 nm, 58 meV at 4.6 nm and 73 meV at 5.6 and 7.0 nm. The root-mean-square deviation over the nine points is 47 meV with the Kane mass and 41 meV with a parabolic mass, so the nonparabolic correction does not improve the agreement at these sizes. The finite barrier is essential: an infinite barrier with parabolic bands gives a root-mean-square deviation of 1128 meV and requires a diameter of 3.9 nm to reproduce the 480 nm peak that the experimental curve assigns to 2.2 nm.

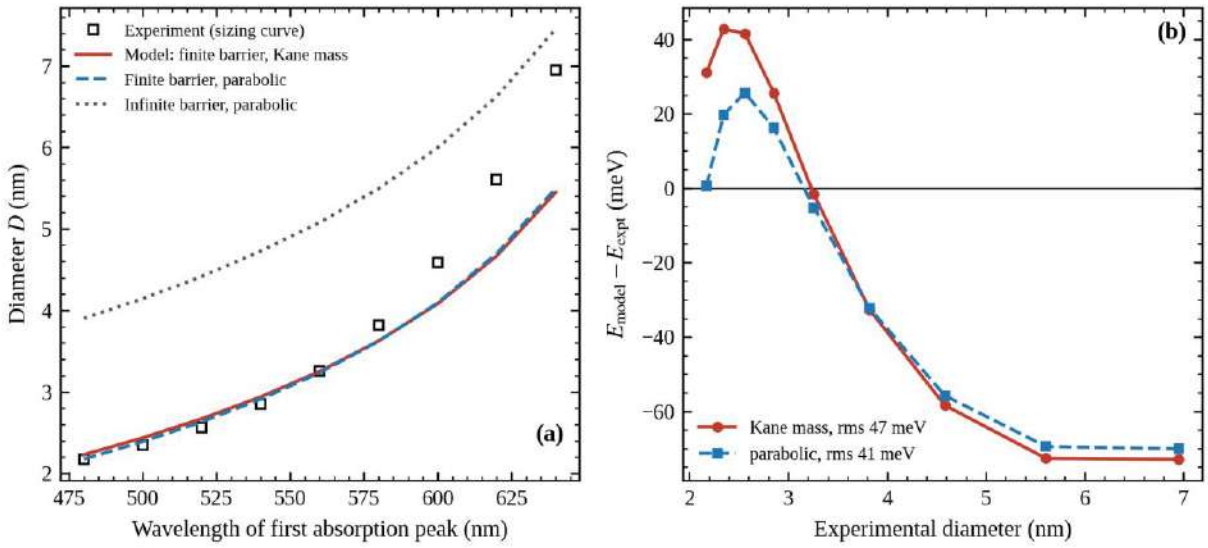


Figure 8. (a) Diameter as a function of the wavelength of the first absorption peak: experimental sizing relation [24] and three models. (b) Difference between model and experimental transition energies as a function of the experimental diameter, for the Kane-mass and parabolic finite-barrier models.

Table 8. Comparison of the calculated lowest transition of CdSe with the experimental sizing relation.

λ (nm)	*D* expt. (nm)	*E* expt. (eV)	*E* model (eV)	Δ*E* (meV)	*D* model (nm)
480	2.17	2.583	2.614	+31	2.23
500	2.34	2.480	2.523	+43	2.44
520	2.56	2.384	2.426	+42	2.67
540	2.85	2.296	2.322	+26	2.94
560	3.26	2.214	2.212	−2	3.25
580	3.82	2.138	2.105	−33	3.63
600	4.58	2.066	2.008	−58	4.08
620	5.61	2.000	1.927	−73	4.67
640	6.95	1.937	1.864	−73	5.45

Experimental values from the sizing relation of Yu et al. [24]; model values computed in this work with the Kane mass. "D model" is the diameter at which the model gives the experimental energy.

The residual changes sign at about 3.3 nm and is not random: it is positive below that size and negative above it. In terms of diameter, the model reaches the experimental energy at a diameter that is 0.9 nm too small at 5.6 nm and 1.5 nm too small at 7.0 nm. Since the barrier was chosen by a scan against the same curve, the small-size agreement within about 40 meV is a consequence of the calibration, while the systematic trend at larger size is the information that the comparison adds.

4.9 Spatial structure of the states

Figure 9 maps the probability density of the electron and hole states of a 4 nm CdSe particle on a plane through its centre, from the radial functions of Section 3.3 multiplied by the spherical harmonics Y_{l0}. The 1S densities are spherical, with the maximum at the centre of the density map and a shell-like radial distribution when weighted by r^2 (Figure 2b). The 1P and 1D states have one and two nodal planes through the

centre and concentrate density in lobes along the symmetry axis near the surface, where the leakage into the barrier is largest. The 2S state has a spherical node at 1.2 nm and a bright core. The electron states (0.30, 0.62, 0.97 and 1.15 eV) extend visibly beyond the dashed boundary, whereas the hole states (0.15, 0.29, 0.45 and 0.53 eV) are held more tightly inside it. The overlap between electron and hole states of the same symmetry is close to unity, which is why the transitions listed in Table 7 carry most of the oscillator strength in this model.

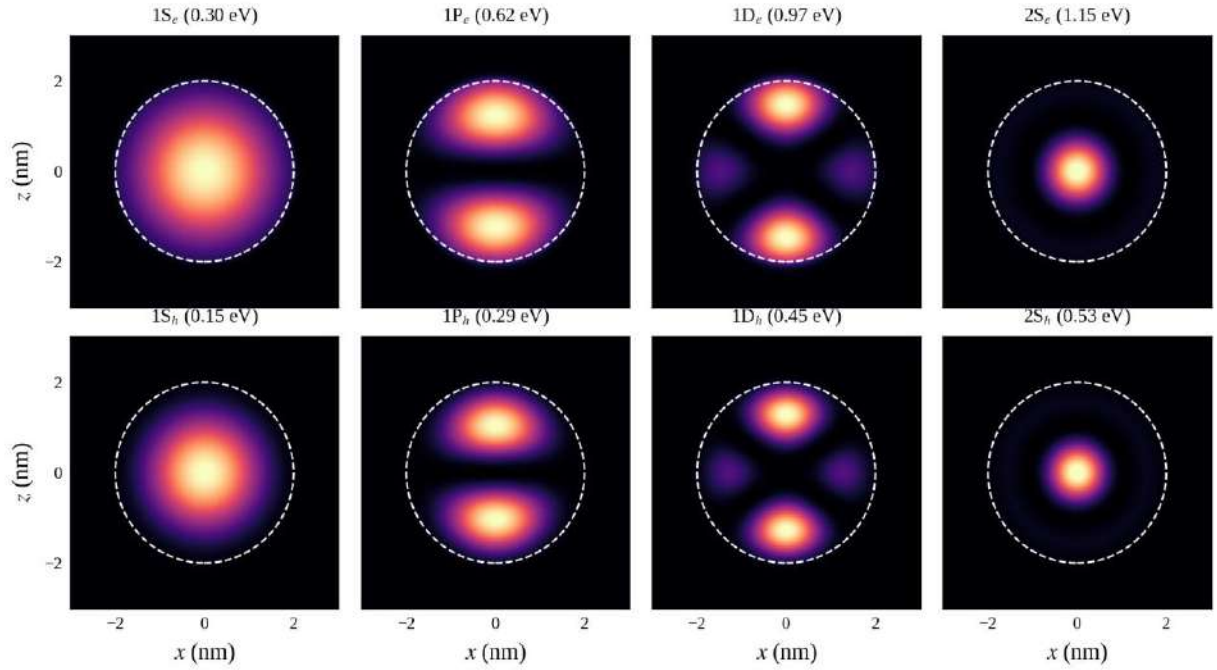


Figure 9. Probability density $|\psi|^2$ in the x–z plane through the centre of a 4 nm CdSe particle for the electron states 1S, 1P, 1D and 2S (top row) and the corresponding hole states (bottom row), with the quantum number of each state and its energy above the band edge in the panel titles. The dashed circle is the particle surface. Each map is scaled to its own maximum.

4.10 Parameter maps and response surfaces

The dependence of the lowest transition on the two interface parameters chosen in Section 3.6 is shown as maps in Figure 10a,b and as surfaces in Figure 11. At a diameter of 3 nm the transition is 2.04 eV for V_0 = 0.5 eV, 2.28 eV for 2 eV and 2.43 eV for 5 eV; at 4 nm, going from 0.5 to 6 eV raises it from 1.94 to 2.18 eV. The contours are steep at small diameter and low barrier and become nearly vertical above 6 nm, so that above that size the transition is controlled by the diameter and not by the barrier. In the same way, the dielectric constant of the Coulomb term (Figure 10b) shifts the 4 nm transition from 1.98 eV at ε = 5 to 2.11 eV at ε = 14, a spread of 0.13 eV, and the 6 nm transition from 1.84 to 1.93 eV, a spread of 0.09 eV. The two choices made against the experimental curve, V_0 = 2 eV and ε = 9.7, therefore lie in a region where the gap changes by about 0.1 eV over the plausible range of either parameter at 4 nm, and a different pair of values on the same curve of equal root-mean-square error would give a similar fit at one size and a different one at another.

Figure 10c is a map of the absorption spectrum as a function of diameter. Each transition appears as a band that moves to lower energy as the particle grows, the bands are separated by gaps that close with size, and the width of each band increases with its slope because a fixed relative size dispersion of 5% produces a width proportional to dE/dD. The bands of higher transitions are therefore broader, which is the reason why the excited transitions in measured spectra of a

polydisperse sample merge at higher energy before the lowest transition does. The surfaces in Figure 11 show the same information in three dimensions together with the probability of finding the electron outside the particle. At 2 nm this probability falls from 38% for V_0 = 0.5 eV to 3.3% for 6 eV, and at 4 nm from 14% to 1.1%. At 10 nm and V_0 = 0.5 eV it is still 3.2%. The leakage surface decreases monotonically in both variables, whereas the gap surface rises with the barrier, so a shell that raises the barrier both blue-shifts the lowest transition and reduces the sensitivity of the carriers to the surface.

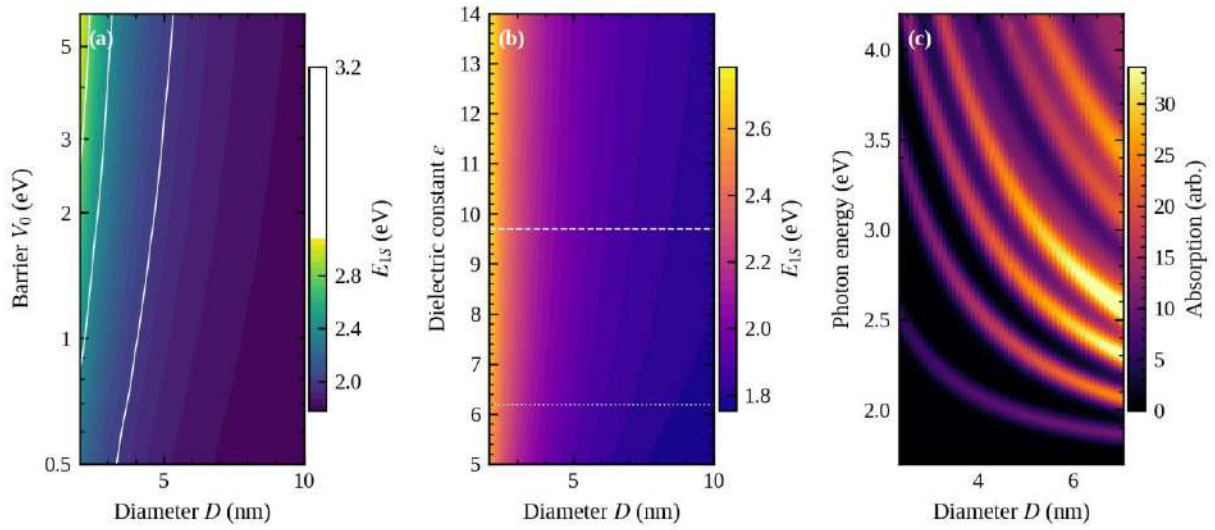


Figure 10. (a) Lowest transition of CdSe as a function of diameter and barrier height, with contours at 2.0, 2.4, 2.8 and 3.2 eV. (b) Lowest transition as a function of diameter and of the dielectric constant of the Coulomb term; the dashed and dotted lines mark the static (9.7) and optical (6.2) values. (c) Map of the model absorption spectrum as a function of diameter, with a 35 meV homogeneous width and a 5% relative size dispersion.

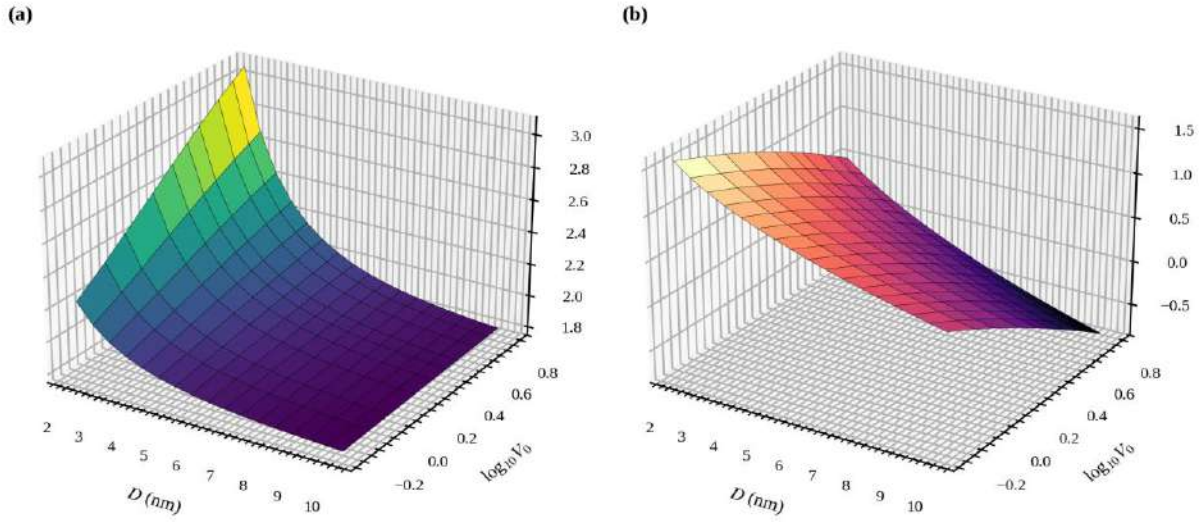


Figure 11. (a) Surface of the lowest transition energy of CdSe as a function of diameter and of the logarithm of the barrier height (in eV). (b) Surface of the logarithm of the percentage probability of finding the 1S electron outside the particle over the same variables.

4.11 Atomistic view of the particle

To relate the continuum diameter to the number of atoms, a wurtzite CdSe lattice with a = 0.430 nm, c = 0.701 nm and the internal parameter u = 0.375 was generated and all sites inside a sphere centred on a Cd atom were counted (Figure 12). A particle of 2, 3, 4, 6 and 8 nm contains 147, 501, 1175, 3989 and 9539 atoms, within 2% of the continuum estimate of 149, 504, 1195, 4032 and 9558 from the volume per CdSe pair of 0.0561 nm^3 that is used in Section 5.7. An atom was counted as under-coordinated when it has fewer than four neighbours within 0.30 nm. The fraction of such atoms in an ideal, unrelaxed and unpassivated sphere is 52% at 2 nm, 37% at 3 nm, 28% at 4 nm, 19% at 6 nm and 14% at 8 nm. It follows roughly the same trend as the leakage of the electron density: the more of the particle that is at the surface, the larger the share of the carrier density that overlaps the interface. In a real particle the surface is reconstructed and passivated by ligands, so these numbers show the geometric limit and not the density of surface states.

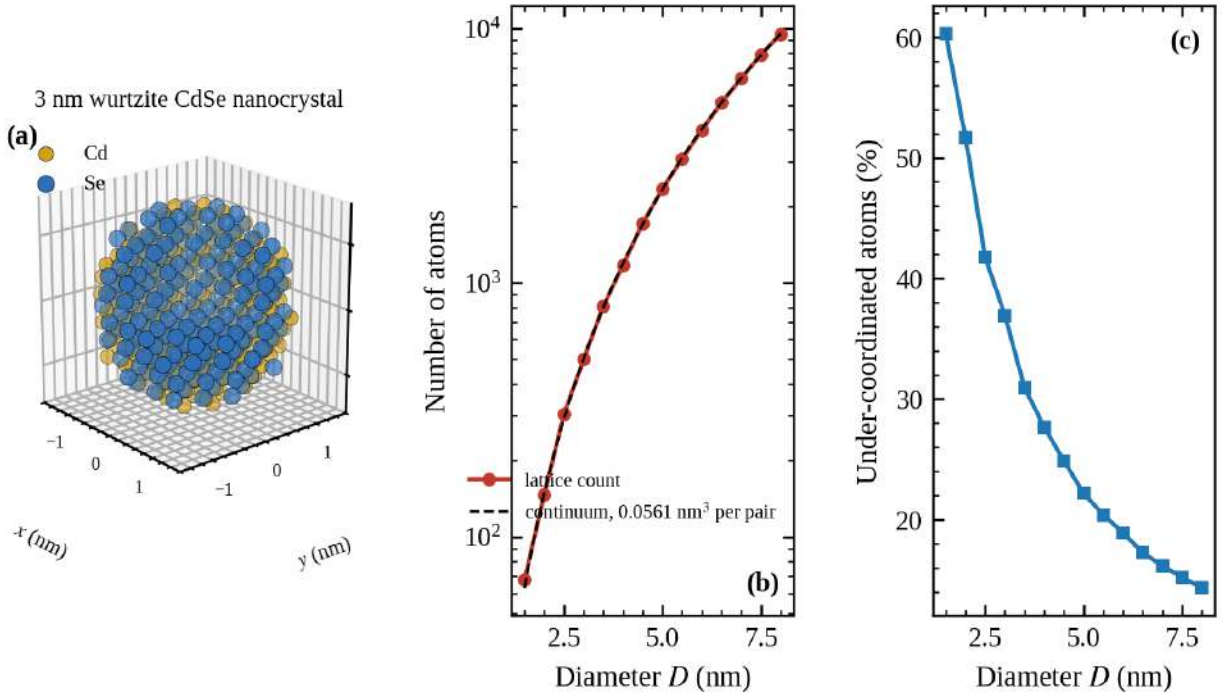


Figure 12. (a) Wurtzite lattice of a CdSe nanocrystal of 3 nm diameter generated for this work (Cd gold, Se blue; ideal geometry, no relaxation or ligands). (b) Number of atoms as a function of diameter from a count of lattice sites, compared with the continuum estimate. (c) Percentage of atoms with fewer than four neighbours within 0.30 nm.

5. Discussion

5.1 Answers to the research questions

RQ1. In CdSe the electron supplies about two thirds of the confinement energy and the hole one third, and the Coulomb attraction removes between 17% and 45% of the confinement energy as the diameter grows from 2 to 10 nm (Table 6). The infinite-barrier model with the same Coulomb term overestimates the shift from the bulk gap by 79% at 4 nm and by 68 to 86% over 3 to 6 nm, because the carriers spend a few per cent of their time outside the particle (Section 4.7). The error is a property of the boundary condition and does not depend on the quality of the band parameters.

RQ2. The finite-barrier continuum model reproduces the CdSe sizing curve to within 43 meV for diameters up to 3.3 nm and then underestimates the transition by an amount that grows to 73 meV at 5.6 to 7 nm, with an overall

root-mean-square deviation of 47 meV. Because two parameters were selected against this curve, the agreement is an upper bound on the predictive accuracy of the model for CdSe, and the accuracy for the other materials is untested here.

RQ3. The sensitivity of the wavelength to size is controlled by the bulk gap and by the size itself, through $d\lambda/dD$, and ranges from 118 nm per nm for InP at 2.5 nm to 3 nm per nm for CdS at 8 nm. A result for the gap should be reported together with the diameter and its distribution, the barrier or medium assumed, the dielectric constant used in the Coulomb term, and the mass model, because each of these changes the 4 nm transition of CdSe by tens to hundreds of millielectronvolts.

5.2 Why the barrier matters more than the band structure

The two band-structure corrections tested here are small compared with the barrier. Replacing the Kane mass by a parabolic one changes the 1S transition of CdSe by 40 meV at 2 nm, by 7 meV at 3 nm and by less than 4 meV from 4 to 10 nm, whereas replacing the finite barrier by an infinite one changes it by 0.27 eV at 4 nm. The reason is that the carriers have low masses and small confinement energies compared with the 2 eV barrier, so that the condition on the logarithmic derivative at the interface depends on the ratio of the penetration depth to the radius. With $\kappa = 0.67$ Å^{-1} for the electron at the energy of the 1S state, the penetration depth $1/\kappa$ is 0.15 nm, which is 7.5% of the radius of a 4 nm particle. This is a general feature: any improvement of the intrinsic description of the band, such as the use of more bands, is secondary to a correct statement of the surroundings for particles in this size range [11, 23]. It also means that two samples of the same material and size can have optical gaps that differ by more than the nominal size effect when the ligand or shell is changed, as is used deliberately in core–shell design [18].

5.3 The Coulomb term and the intermediate regime

The first-order treatment of the electron–hole attraction is justified when the Coulomb energy is small compared with the spacing of the confinement levels. In CdSe at 4 nm the Coulomb energy of 0.107 eV is smaller than the electron 1S–1P spacing of 0.32 eV, but it is not small compared with the hole spacing of 0.14 eV. The hole is therefore not strictly in the strong-confinement regime (a_h = 1.1 nm against R = 2 nm), and the neglect of the mixing of hole levels by the electron field could be significant [11, 29]. The choice of the dielectric constant moves the 4 nm transition by about 0.1 eV (the Coulomb energy is 0.107 eV with $\varepsilon_s = 9.7$ and 0.17 eV with $\varepsilon_\infty = 6.2$, by the $1/\varepsilon$ scaling of Eq. 4). We chose the static value because the scan against the CdSe curve favoured it, not because the physics demands it. Atomistic calculations of the exciton Coulomb energy offer a way to settle the question without a fit [21].

5.4 The deviation at larger sizes

The systematic underestimate of the transition energy above 3.3 nm means that the model gives too little confinement at those sizes, or too much Coulomb attraction. The data do not identify the cause. Several candidates are consistent with the trend. The first is the hole mass: the heavy-hole mass of 0.45 m_0 is a band-edge value for one direction and the valence band of CdSe is anisotropic and split by the wurtzite crystal field, so that the effective mass for confinement can differ [10, 11]. A larger hole mass lowers the hole confinement energy, which would worsen the agreement, whereas a smaller one would improve it; the sign of the correction is thus an open question that a multi-band calculation could answer. The second is the use of the room-temperature bulk gap of 1.74 eV with sizing data collected for particles whose surfaces and strain may differ from the bulk. The third is the polarisation energy at the interface, which was neglected. Only a calculation that includes these effects can distinguish among them, and we do not claim a cause.

5.5 Implications for devices and for reporting

For emission at a chosen wavelength the model gives a starting diameter and the size control required. For CdSe at 4 nm a diameter error of 0.1 nm shifts the transition by about 4 nm, and the 5% dispersion typical of good syntheses [9] already produces about 19 nm of inhomogeneous width.

For wavelength targets in the red and near infrared, InP and CdTe offer larger tuning ranges but also more sensitivity, so they need tighter size control for the same linewidth. For gain and lasing applications, the spacing between the first and second absorption transitions, 0.48 eV for CdSe at 4 nm, sets how well the band-edge state can be isolated from the next level [13]. Based on the findings, we recommend that papers on confinement report (i) the diameter, its standard deviation and the method used to measure it; (ii) the bulk parameters used, including the mass of each carrier and the temperature of the gap; (iii) the barrier height and the mass outside the particle, or the statement that an infinite barrier was used; (iv) the dielectric constant of the Coulomb term; (v) whether nonparabolicity and valence-band mixing were included; and (vi) the comparison with experiment as a function of diameter, not at a single size.

5.6 Limitations

The main limitations are as follows. The model is continuum and spherical: it cannot describe surface reconstruction, facets, ligands or defects, and real particles are often elongated or faceted. The barrier is rectangular, identical for electrons and holes and identical across materials, which is a simplification, because the band offsets to a ligand shell or a wider-gap shell differ by carrier and by material. The valence band is a single heavy-hole band, so the fine structure and the order of the higher transitions, which depend on valence-band mixing, cannot be predicted [10]. The Coulomb term is evaluated to first order and with a bulk dielectric constant, and polarisation of the medium and electron–hole exchange are omitted. The experimental comparison uses a published fit and not primary data, covers one material and one range of sizes, and shares information with the calibration of the two parameters. The results for CdS, CdTe, ZnSe and InP have not been tested against measurements in this work. Finally, and importantly, no density functional or other atomistic calculation was done, so statements about the accuracy of such methods in Section 2.3 come from the literature and not from this study.

5.7 Future work

The next step is to repeat the calculation for the same particles with an atomistic method. A plane-wave density functional calculation [34, 35] of passivated CdSe particles has a cost that scales steeply with the number of atoms: a spherical wurtzite particle of 2, 3, 4, 6 and 8 nm diameter contains about 150, 500, 1200, 4000 and 9600 atoms (from a cell volume of 0.0561 nm^3 per CdSe pair, confirmed by a direct count of lattice sites in Section 4.11), so the range in which the present model shows the largest deviations lies beyond routine calculations with standard functionals. A practical route is to use density functional theory with a screened hybrid functional [31] for particles up to about 3 nm and to compare the size dependence of the gap, the level spacings and the wavefunction leakage with Table 4 and Figure 7, and then to use an empirical pseudopotential or tight-binding model [20, 21, 30] for the larger sizes, calibrated on the smaller ones. A parallel line of work is to include valence-band mixing in the continuum model, to treat a shell with its own band offsets, and to compare with spectra measured on samples whose size distribution has been determined independently.

6. Conclusion

We solved the quantum-mechanical envelope-function problem for spherical CdS, CdSe, CdTe, ZnSe and InP particles with a finite barrier, an energy-dependent mass and a Coulomb correction computed from the wavefunctions, and tested the root finder against an independent finite-difference solution to 0.2 meV. For CdSe the lowest transition ranges from 1.83 eV at 8 nm to 2.73 eV at 2 nm. At 4 nm the electron and hole confinement energies are 0.30 and 0.15 eV, the Coulomb term removes 0.11 eV and the net shift from the bulk gap is 0.34 eV. The infinite-barrier model overestimates the shift by 68 to 86% between 3 and 6 nm because 2 to 6% of the electron density lies outside the particle, while the use of the Kane mass in place of a parabolic one changes the gap by 40 meV at 2 nm and by less than 7 meV from 3 nm upward. The model matches a published CdSe sizing curve with a root-mean-square deviation of 47 meV after two interface parameters were selected against it, and

it underestimates the transition by up to 73 meV above 3.3 nm for reasons that this level of theory cannot resolve. The sensitivity of the transition wavelength to diameter, from 3 to 118 nm per nm across the materials and sizes studied, sets the size control needed for a target linewidth. These results show which parts of the confinement problem a continuum model settles and which parts, namely the surface, the valence-band structure and the screening of the Coulomb interaction, need an atomistic first-principles treatment, which we have outlined and not carried out.

REFERENCES

[1] Ekimov AI, Onushchenko AA. Quantum size effect in three-dimensional microscopic semiconductor crystals. JETP Lett. 1981;34(6):345–349.

[2] Ekimov AI, Efros AlL, Onushchenko AA. Quantum size effect in semiconductor microcrystals. Solid State Commun. 1985;56(11):921–924.

[3] Efros AlL, Efros AL. Interband absorption of light in a semiconductor sphere. Sov Phys Semicond. 1982;16(7):772–775.

[4] Rossetti R, Nakahara S, Brus LE. Quantum size effects in the redox potentials, resonance Raman spectra, and electronic spectra of CdS crystallites in aqueous solution. J Chem Phys. 1983;79(2):1086–1088.

[5] Brus LE. Electron–electron and electron–hole interactions in small semiconductor crystallites: the size dependence of the lowest excited electronic state. J Chem Phys. 1984;80(9):4403–4409.

[6] Brus L. Electronic wave functions in semiconductor clusters: experiment and theory. J Phys Chem. 1986;90(12):2555–2560.

[7] Bawendi MG, Steigerwald ML, Brus LE. The quantum mechanics of larger semiconductor clusters ("quantum dots"). Annu Rev Phys Chem. 1990;41:477–496.

[8] Alivisatos AP. Semiconductor clusters, nanocrystals, and quantum dots. Science. 1996;271(5251):933–937.

[9] Murray CB, Norris DJ, Bawendi MG. Synthesis and characterization of nearly monodisperse CdE (E = S, Se, Te) semiconductor nanocrystallites. J Am Chem Soc. 1993;115(19):8706–8715.

[10] Norris DJ, Bawendi MG. Measurement and assignment of the size-dependent optical spectrum in CdSe quantum dots. Phys Rev B. 1996;53(24):16338–16346.

[11] Efros AlL, Rosen M. The electronic structure of semiconductor nanocrystals. Annu Rev Mater Sci. 2000;30:475–521.

[12]Colvin VL, Schlamp MC, Alivisatos AP. Light-emitting diodes made from cadmium selenide nanocrystals and a semiconducting polymer. Nature. 1994;370(6488):354–357.

[13] Klimov VI, Mikhailovsky AA, Xu S, Malko A, Hollingsworth JA, Leatherdale CA, et al. Optical gain and stimulated emission in nanocrystal quantum dots. Science. 2000;290(5490):314–317.

[14] Michalet X, Pinaud FF, Bentolila LA, Tsay JM, Doose S, Li JJ, et al. Quantum dots for live cells, in vivo imaging, and diagnostics. Science. 2005;307(5709):538–544.

[15] Canham LT. Silicon quantum wire array fabrication by electrochemical and chemical dissolution of wafers. Appl Phys Lett. 1990;57(10):1046–1048.

[16] Kovalenko MV, Manna L, Cabot A, Hens Z, Talapin DV, Kagan CR, et al. Prospects of nanoscience with nanocrystals. ACS Nano. 2015;9(2):1012–1057.

[17] García de Arquer FP, Talapin DV, Klimov VI, Arakawa Y, Bayer M, Sargent EH. Semiconductor quantum dots: technological progress and future challenges. Science. 2021;373(6555):eaaz8541.

[18] Reiss P, Protière M, Li L. Core/shell semiconductor nanocrystals. Small. 2009;5(2):154–168.

[19] Perdew JP, Levy M. Physical content of the exact Kohn–Sham orbital energies: band gaps and derivative discontinuities. Phys Rev Lett. 1983;51(20):1884–1887.

[20] Wang LW, Zunger A. Solving Schrödinger's equation around a desired energy: application to silicon quantum dots. J Chem Phys. 1994;100(3):2394–2397.
[21] Franceschetti A, Zunger A. Direct pseudopotential calculation of exciton Coulomb and exchange energies in semiconductor quantum dots. Phys Rev Lett. 1997;78(5):915–918.
[22] BenDaniel DJ, Duke CB. Space-charge effects on electron tunneling. Phys Rev. 1966;152(2):683–692.
[23] Bastard G. Wave Mechanics Applied to Semiconductor Heterostructures. Les Ulis: Les Éditions de Physique; 1988.
[24] Yu WW, Qu L, Guo W, Peng X. Experimental determination of the extinction coefficient of CdTe, CdSe, and CdS nanocrystals. Chem Mater. 2003;15(14):2854–2860.
[25] Hohenberg P, Kohn W. Inhomogeneous electron gas. Phys Rev. 1964;136(3B):B864–B871.
[26] Kohn W, Sham LJ. Self-consistent equations including exchange and correlation effects. Phys Rev. 1965;140(4A):A1133–A1138.
[27] Kittel C. Introduction to Solid State Physics. 8th ed. Hoboken: Wiley; 2005.
[28] Kane EO. Band structure of indium antimonide. J Phys Chem Solids. 1957;1(4):249–261.
[29] Kayanuma Y. Quantum-size effects of interacting electrons and holes in semiconductor microcrystals with spherical shape. Phys Rev B. 1988;38(14):9797–9805.
[30] Delerue C, Allan G, Lannoo M. Theoretical aspects of the luminescence of porous silicon. Phys Rev B. 1993;48(15):11024–11036.
[31] Heyd J, Scuseria GE, Ernzerhof M. Hybrid functionals based on a screened Coulomb potential. J Chem Phys. 2003;118(18):8207–8215.
[32] Hedin L. New method for calculating the one-particle Green's function with application to the electron-gas problem. Phys Rev. 1965;139(3A):A796–A823.
[33] Rohlfing M, Louie SG. Electron–hole excitations and optical spectra from first principles. Phys Rev B. 2000;62(8):4927–4944.
[34] Kresse G, Furthmüller J. Efficient iterative schemes for ab initio total-energy calculations using a plane-wave basis set. Phys Rev B. 1996;54(16):11169–11186.
[35] Giannozzi P, Baroni S, Bonini N, Calandra M, Car R, Cavazzoni C, et al. QUANTUM ESPRESSO: a modular and open-source software project for quantum simulations of materials. J Phys Condens Matter. 2009;21(39):395502.
[36] Madelung O, editor. Semiconductors: Data Handbook. 3rd ed. Berlin: Springer; 2004.
[37] Vurgaftman I, Meyer JR, Ram-Mohan LR. Band parameters for III–V compound semiconductors and their alloys. J Appl Phys. 2001;89(11):5815–5875.

IEER
Institute for Excellence in Education & Research